Journal of Food Engineering 291 (2021) 110289

Contents lists available at ScienceDirect

Journal of Food Engineering

journal homepage: http://www.elsevier.com/locate/jfoodeng

Measuring internal quality traits in egg by 3D laser imaging

Kaveh Mollazade [a,b,*], Sven Jörissen [b], Andreas Nüchter [b]

[a] Department of Biosystems Engineering, Faculty of Agriculture, University of Kurdistan, Sanandaj, Iran
[b] Informatics VII: Robotics and Telematics, Julius-Maximilians-University Würzburg, Am Hubland, Würzburg, 97074, Germany

ARTICLE INFO

Keywords:
Freshness
Haugh unit
Image processing
Laser scanning
Yolk index

ABSTRACT

Quality of the egg is examined before the production process in the food industry. In this study, a 3D laser scanning approach was developed to measure internal quality traits of the egg. Experiments were carried out on 450 chicken egg samples in different freshness stages. Spectroscopic analysis showed 600–700 nm would be a suitable wavelength region for laser scanning. The quasi-liquid transparency nature of the albumin introduced issues to laser scanning, which were fixed by two solutions: 1. coating of the thick albumin region with Talcum powder before scanning, and 2. training a multilayer perceptron neural network to map the 2D shape features of the thick albumin region to the actual albumin height values. Results indicated that the yolk index and Haugh unit are reliably measured using 3D scanning of the yolk part (R = 0.97 and RMSE = 0.04) and the 2D shape analysis of the thick albumin region (R = 0.84 and RMSE = 6.53), respectively.

1. Introduction

The chicken egg has a high biological value since it contains vitamins, minerals, and essential unsaturated fatty acids (Aygun and Sert, 2013). Due to its unique compounds and its special properties, such as volatility, emulsifying, and specific color and flavor, it is widely used in the formulation of a variety of food products such as dairy products, confectionery, sauces, and fast foods (Abeyrathne et al., 2013). In addition to food applications, due to having bioactive compounds, there is a large potential market for functional egg products in the health and medical sectors (Miranda et al., 2015). Egg quality is essential for the economic success of food producers who use it in their products; because the loss of weight and quality occurs in this foodstuff over time and will cause deterioration.

Usually, in the analytical laboratory of food processing industries, egg quality is examined before the use in the production process. Quality of the egg is investigated for both internal and external characteristics. External quality traits focus on eggshell and are mainly related to the existence of a cracked shell or stains. On the other hand, internal traits are dependent on the egg content, i.e., the quality of the albumin and yolk parts. The most widely used internal egg quality traits are albumin pH, size of the air chamber, height of the albumin, Haugh unit, and yolk index (Abdel-Nour, 2008). While some non-destructive methods, like hyperspectral imaging, have been developed for determining the freshness of egg (Zhang et al., 2015; Suktanarak and Teerachaichayut, 2017; Yao et al., 2020), the breaking and the manual measurement method is still used in many places as the standard method. Manual measurement is not only time-consuming, but also more subjective and open to inconsistent results caused by human error. Therefore, the use of an automated approach would not only increase the speed of measurement, but would also eliminate operator-generated errors.

Today, ultrasonic devices are commercially available for determining the freshness of egg via measuring the albumin height and calculating the Haugh unit. Literature shows that no scientific report has been published so far as to their accuracy. On the other hand, no attempt has yet been made to provide a machine-based solution for measuring the other egg freshness indicators, i.e., yolk index and air cell height. Three-dimensional (3D) vision, as an emerging and developing technology, seems to be a useful tool for simultaneous measuring egg internal quality traits, and more importantly, analyzing the changes in the shape of albumin, yolk, and air cell chamber. In addition to being non-contact, 3D vision systems can scan the scene in a short time and record the spatial information of objects in x, y, and z directions. Literature review demonstrates that extensive research has been carried out during the last decade on the development and implementation of 3D imaging techniques both in science and engineering (Lazaros et al., 2008; Tippetts et al., 2016). Recently, these techniques are being used in many applications for studying shape analysis of agro-food materials. In general, in the analysis of the shape of objects, attention is drawn to the two-dimensional (2D) or 3D features. Accordingly, for the analysis of the

* Corresponding author. Department of Biosystems Engineering, Faculty of Agriculture, University of Kurdistan, Sanandaj, Iran.
E-mail address: k.mollazade@uok.ac.ir (K. Mollazade).

https://doi.org/10.1016/j.jfoodeng.2020.110289
Received 2 April 2020; Received in revised form 8 August 2020; Accepted 10 August 2020
Available online 13 August 2020
0260-8774/© 2020 Elsevier Ltd. All rights reserved.

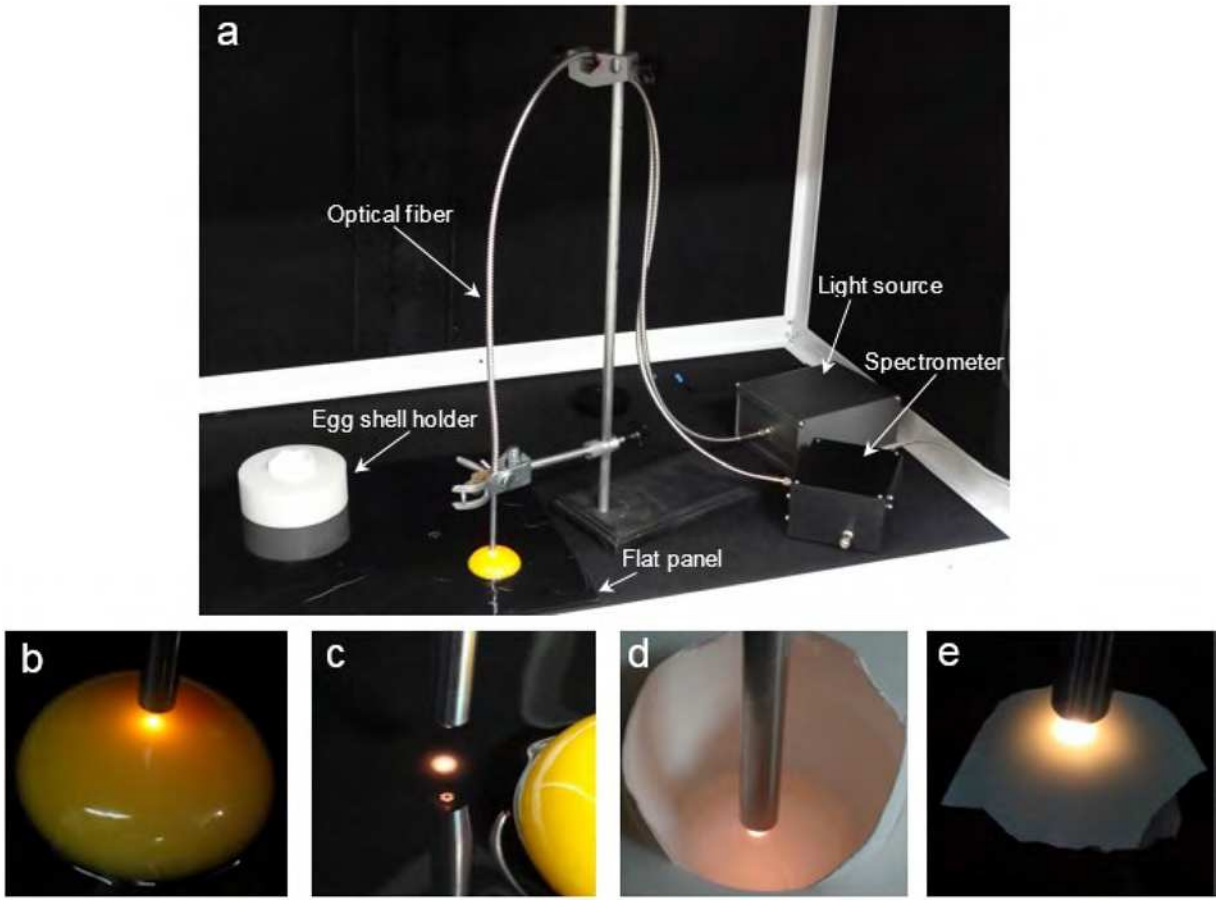

Fig. 1. Spectroscopy setup (a) and spectra collection procedure for yolk (b), albumin (c), air cell (d), and eggshell (e).

shape of objects, either 2D characteristics of the area, perimeter, eccentricity, boundary information of the object, etc., or 3D features of the reconstructed shape and the volume are considered as the desirable parameter. For example, Sakai and Yonekawa (1992) used a 3D laser-based triangulation technique to extract contours of soybean shape and express the surface area and volume as functions of seed mass.

The existing techniques for extracting 3D information from 2D images are divided into active and passive categories. In active methods, the 3D information is extracted by diffusion of optical patterns, usually laser light, on the surface of the desired object and then the analysis of the reflected light, while in passive methods, the only the analysis of acquired images is considered (Ivorra et al., 2015). As reported in several studies, the use of structured light forms the main basis of active methods (Verdú et al., 2013; Zou and Chen, 2018). The simplest way to implement the structured light method is by recording the reflection of a laser line on the desired surface and its respective movement over the object. Thus, the contour of the object can be reconstructed by analyzing the distortion of the shape of the reflection of the laser. Volume measurement of oyster meat (Lee et al., 2001), weight estimation of herring (Mathiassen et al., 2011), plant phenotyping (Kjaer and Ottosen, 2015), and quality grading of Atlantic salmon (Sture et al., 2016) are examples of the application of active 3D vision methods in agriculture and food industry.

This research aims to demonstrate the development of a non-contact approach based on 3D laser imaging to measure the internal quality traits of the egg. This is achieved through the following steps:

- Finding the most suitable wavelength region for laser scanning of egg content
- Evaluating the performance of the proposed 3D vision approach with that of the manual method in measuring internal quality traits
- Investigating the feasibility of using 2D shape descriptors of the thick albumin region for the prediction of the thick albumin height and Haugh unit

2. Material and methods

Given the semi-turbid nature of egg content, the laser diode for 3D scanning has to be selected in a wavelength region where not only light reflectance is high (less absorbance) but also the degree of similarity among spectra of different parts of the egg content is maximum. Therefore, spectroscopy tests were first carried out in the visible and short-wavelength near-infrared (Vis-SWNIR) of the electromagnetic spectrum. After that, in another experiment, the 3D laser scanning of eggs was performed.

2.1. Spectroscopy experiment

2.1.1. Sample preparation

For the spectroscopy analysis, a dataset containing Vis-SWNIR spectra of 225 chicken eggs at different freshness stages was prepared. Commercial eggs from the first day of egg-laying were purchased in February 2019 from the Atlas poultry egg production farm near Sanandaj, Iran. The eggs were inspected individually, and the eggs with cracks were removed. On arrival of the eggs at the laboratory, 15 samples were analyzed, and the rest were stored under controlled storage conditions in two equal groups to generate samples with different freshness stages. The first group was kept in a refrigerator (4 ± 1 °C and 75 ± 5% relative humidity), while the other group remained at room

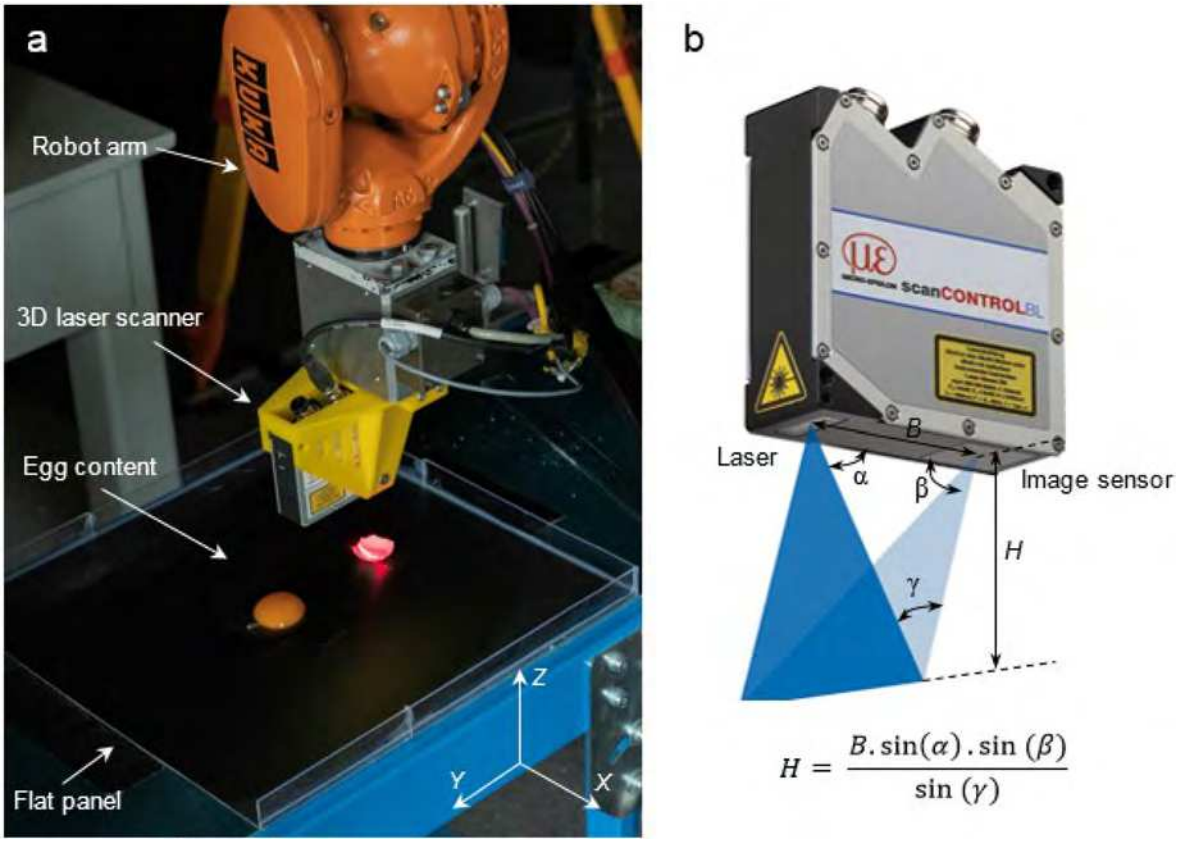

Fig. 2. 3D laser imaging setup (a), and height (H) calculation by triangulation method (b).

conditions (24 ± 1 °C and 40 ± 5% relative humidity). In three-day intervals over the three-week storage period, 15 eggs from each group were selected for analysis. Cold storage samples were placed at ambient temperature 2 h before the beginning of the experiment to allow them to reach the room temperature (24 ± 1 °C) (Aboonajmi et al., 2010).

2.1.2. Device properties

The Vis-SWNIR measurements were performed using a high-resolution spectrometer V900 (OPTC Inc., Kashan, Iran) equipped with a Czerny-Turner optical bench, a Toshiba TCD1304AP detector, and premium grade reflection probes. Spectroscopy was performed in the interactance mode so that its results could be generalized to the 3D laser scanning experiment, in which the laser light reflected from the scene is recorded on camera. Experiments were carried out at ambient temperature. In each experiment stage, the eggs were manually broken out on a smooth black color flat panel. Since albumin is a quasi-liquid transparent material, major parts of incident light pass through and go out of it. The black surface absorbs parts of passed light photons, and thus allowing the rest of photons to return into the albumin without the backscattering effect. The Vis-SWNIR spectra of different parts of eggs, including the yolk, albumin, air cell, and shell were acquired in triplicate in the interactance mode in the range 400–1100 nm. The average value of these three measurements was used as a single sample measurement. Reference white and dark spectra were also acquired at the beginning of each experiment to calculate the relative spectra of the samples by eliminating the optical interferences caused by both light source and spectrometer (Moomkesh et al., 2017). Fig. 1 shows the experimental spectroscopy setup and the spectra collection method.

After data acquisition and reflectance calibration, raw spectra were subjected to the Savitzky-Golay (SG) smoothing algorithm (21 smoothing points, 8th-order) for eliminating the artificial noise caused by the spectrometer. The similarity between the average spectra of different parts of egg content was assessed by calculating the angle (α) between pairs of spectral vectors. The Spectral Angle Mapper (SAM) computes the angle of two spectral vectors with the same wavelength range as following (Ma et al., 2016):

$$SAM = cos^{-1}\left(\frac{S_A.S_b}{|S_A||S_B|}\right) = cos^{-1}\left(\sum_{i=1}^{N}\left(\frac{(S_A)_i(S_B)_i}{\sqrt{\sum_{i=1}^{N}(S_A)_i(S_A)_i}\sqrt{\sum_{i=1}^{N}(S_B)_i(S_B)_i}}\right)\right) \quad (1)$$

where, S_A and S_B are spectral vectors, and N refers to the length of vectors. Here, the smaller the SAM value, the higher the similarity of the two spectral vectors. Since SAM uses vector direction, not vector length, it is free of illumination intensity effects.

2.2. 3D scanning experiment

2.2.1. 3D point cloud acquisition

The sample preparation process and the number of eggs for the 3D scanning experiment were precisely the same as the spectroscopy experiment (section 2.1.1.). Here, samples were prepared in July 2019 from the Endres-Ei GmbH egg production facility near Würzburg, Germany. In each experiment stage, egg samples were first weighed using a digital scale (GundG Taschenwaage, accuracy: 0.01 g), then broken onto a black color flat panel by breakout method. A calibrated high-speed Micro-Epsilon scanControl 2900-25 laser profile scanner was mounted to the flange of a 6-axis KUKA KR16 robot (0.04 mm repeatability) to scan the egg content (yolk, albumin, and air cell). The Micro-Epsilon scanner is equipped with a low power Class 2M semiconductor linear laser (emitting at 658 nm) and a CMOS image sensor (Fig. 2-a). The scanner projects a laser line onto the egg content, and the image sensor collects the reflected laser light. Height information (H) is then calculated by triangulation (Fig. 2-b). The reference resolution of the scanner along the height direction (z-axis) is ±2 μm with a measuring range of

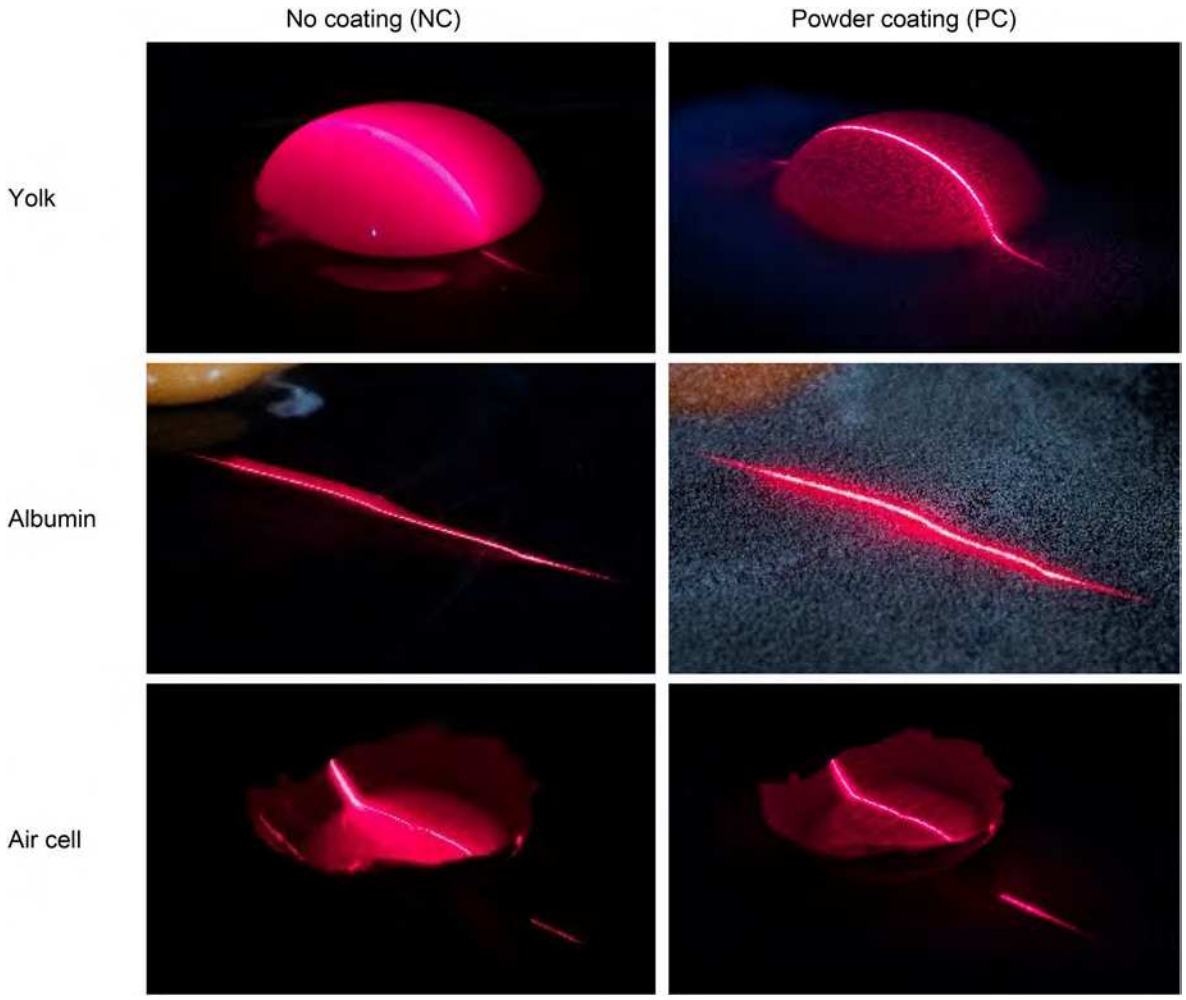

Fig. 3. Laser strip on different parts of egg content in no coating and powder coating modes.

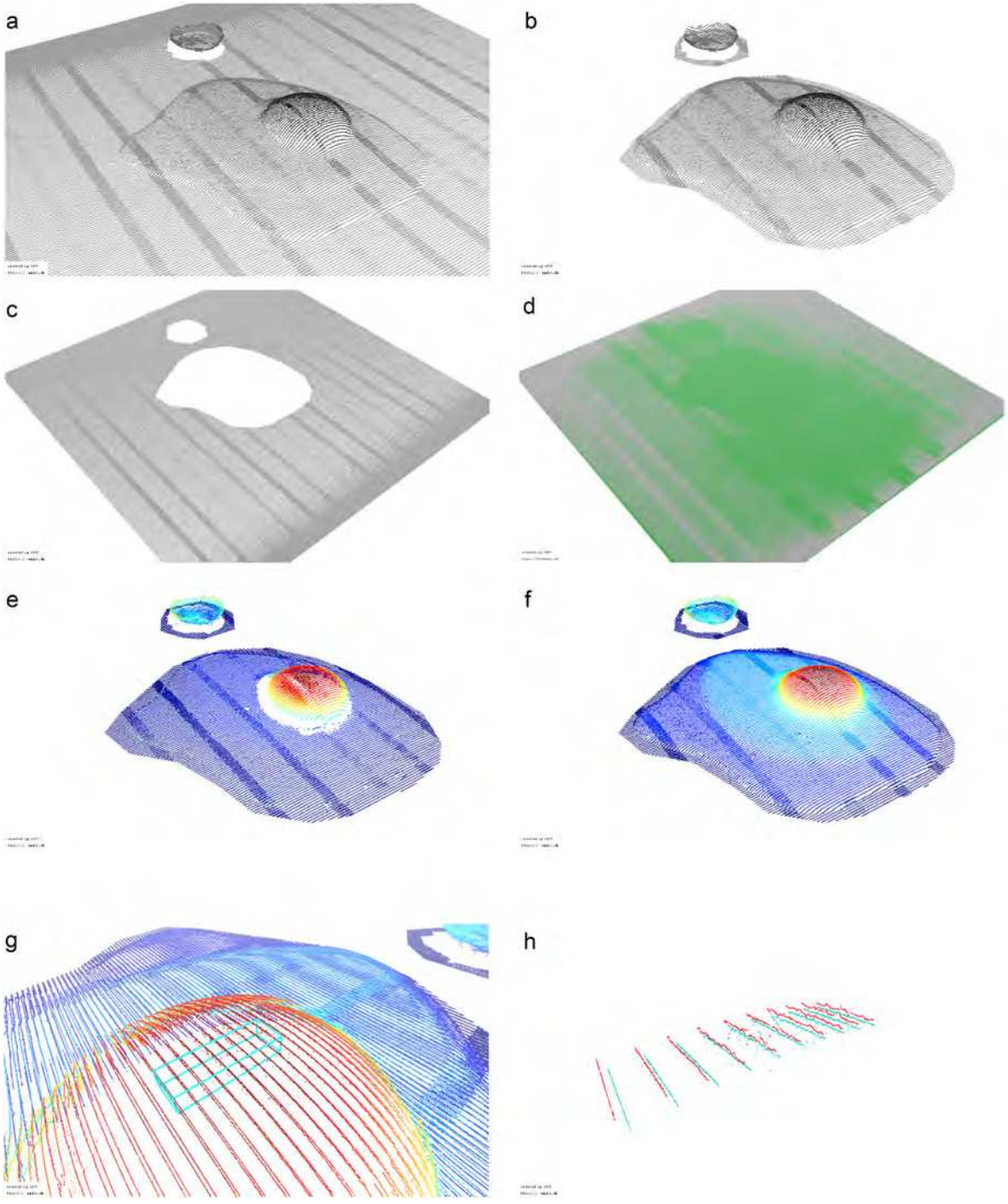

Fig. 4. Point cloud processing: loading the point cloud of NC and PC scans (a), segmentation of egg content parts (b), remained point cloud of flat panel after segmentation (c), fitting a plane onto the point cloud of flat panel (d), and height map of height difference between point clouds of egg content parts and fitted plane (e and f for NC and PC scans, respectively). Note: The strips originate from the scanning process and are a result of the overlap. They have no effect to the evaluation. Sample position of region of interest (ROI) for height extraction from yolk, albumin, and air cell (g, i, and k, respectively), and points extracted from yolk, albumin, and air cell for both NC and PC scans (h, j, and l, respectively). Note: The strips originate from the scanning process and are a result of the overlap. They have no effect to the evaluation.

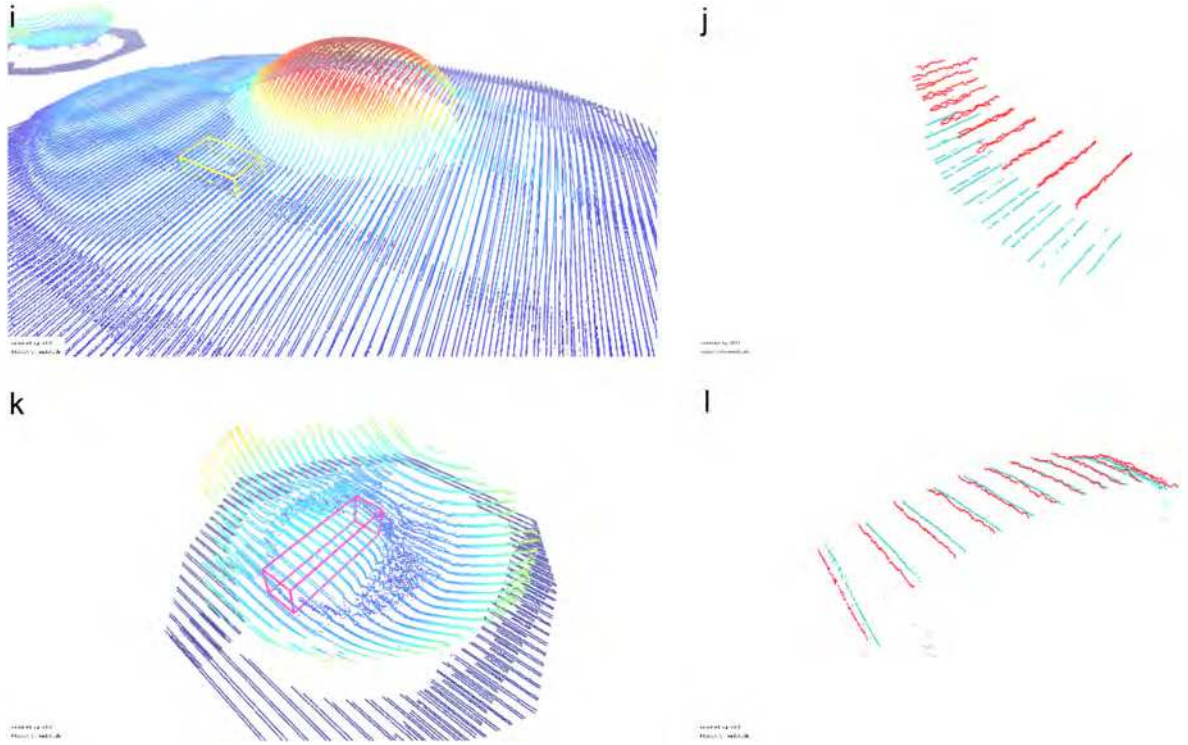

Fig. 4. (*continued*).

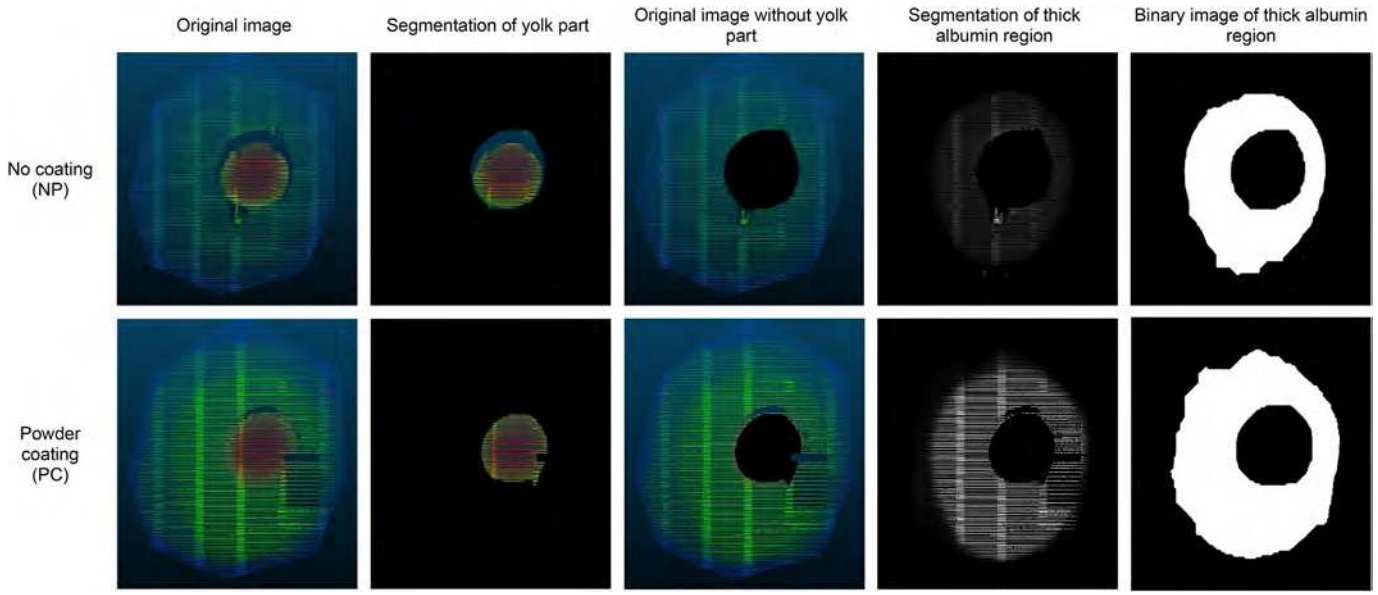

Fig. 5. Analysis of height's 2D BGR images to segment thick albumin region.

25 mm starting at 53.5 mm and ending at 78.5 mm. The scanning width per line (x-axis) ranges from 23.4 mm to 29.1 mm, depending on the aforementioned distances, respectively, with a resolution of 1280 points/profile. Scanner-Base calibration was performed using KUKAs internal *XYZ – 4 Point* and *ABC – 2 Point* methods to determine position and orientation of the Tool Center Point (TCP) with respect to the robot's base coordinate system. To cover the entire scene (35 × 35 cm panel), the KUKA robot was programmed to scan the whole surface with 15 consecutive sweeps with a scan width of 27 mm each to ensure sufficient overlap for various heights during scanning. The acquired data (x, y, and z coordinates of each point scanned by the laser scanner) of each egg sample were stored on a desktop computer in the *ASCII .pts* format for further analysis.

Primary tests revealed that the height of the egg content (especially for albumin) measured by the 3D laser scanning method might not necessarily represent actual values. The reason for this is due to the transparency nature of the albumin. After breaking the egg, a thin layer of albumin remains on the surface of the yolk and the air cell membrane. This thin layer may refract the laser light when it hits the yolk and the air cell membrane surface. As for the albumin itself, laser light passes through it all; and after colliding with the black panel, a portion of the light energy is absorbed and the light coming back into the albumin

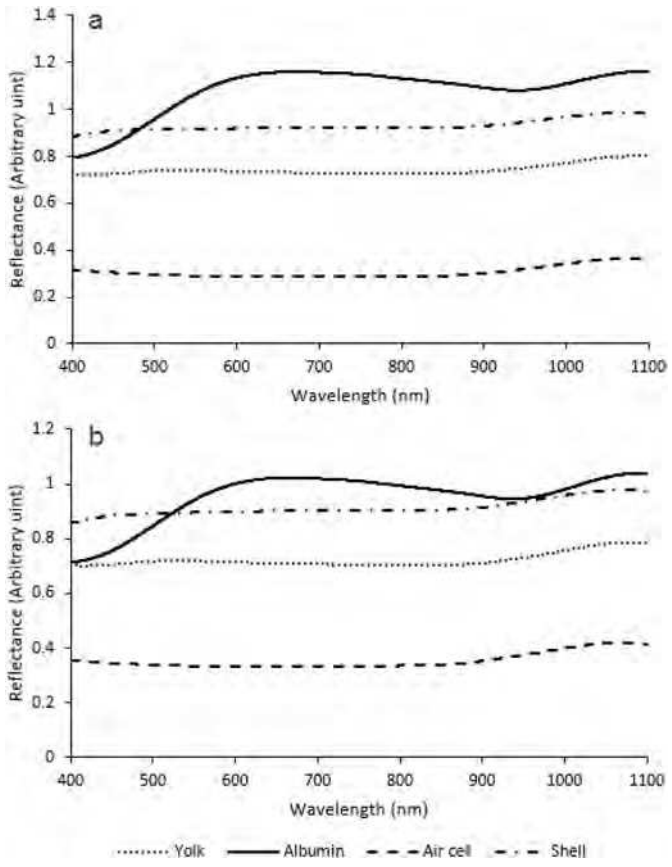

Fig. 6. Average reflectance of the processed spectra of egg samples at room (a) and cold (b) storage conditions.

cannot be returned to its surface due to the energy loss (Fig. 3). Given the above, to have the exact 3D profile of each sample, the surface of all egg sections was covered manually with a thin layer of Talcum powder using a size four coffee filter with a metal mesh grid of about 200 μm. To determine the approximate thickness of the coating, the black surface was scanned both coated and not coated and the point to point distance was calculated, which was generally below 0.1 mm, but rarely above that, due to sparse clusters of Talcum powder. Talcum powder is very light and is also hydrophobic. Therefore, it does not mix with the egg content and remains stable on the surface of the egg after coating. As a result, the laser light returns to the camera well, and it is possible to record the exact height values for different parts of egg content (Fig. 3).

2.2.2. Traits' manual measurements

To assess the manual values before each 3D laser scan, internal quality traits including diameter and height of yolk (average of three measurements), long and short diameter of thick albumin, the height of thick albumin (average of three measurements taken at about 10 mm from the yolk), and air cell height (average of measurement at the middle point and at three equidistant points on the air cell membrane) were measured immediately with a digital Vernier caliper (Preciva, accuracy: ± 0.01 mm) and a digital height gauge (Preciva, accuracy: ± 0.01 mm). The Haugh unit (*HU*) was then calculated using Equation (2), where *H* is the albumin height (mm) and *W* is the egg mass (g). The Yolk index (YI) was also determined by dividing the yolk height by its diameter (Aboonajmi et al., 2010; Huang et al., 2012).

$$HU = 100 \times log_{10}\left(H - 1.7W^{0.37} + 7.57\right) \quad (2)$$

2.2.3. 3D point cloud processing

Processing of the point clouds was done in a multi-step fashion. First, the point clouds of no coating (NC) and powder coating (PC) scans were loaded into the processing environment (Fig. 4-a). Second, segmentation was applied manually to separate panel points from egg and shell points (Fig. 4-b and c). Next, a plane was fitted through the panel points to compensate for small surface irregularities with an RMS fitting error of 0.223 ± 0.012 mm (Fig. 4-d). Finally, for each point of egg and shell, the cloud-to-plane distance was calculated to determine the height from the panel. The points were then colored in a BGR scale (Fig. 4-e and f). Since all points are saved with respect to the robot coordinate system, this also accounts for any global tilt of the panel orientation. The distance is calculated as a Euclidean distance along the fitted planes normal vector.

To get the height values at the desired locations from the acquired point cloud data (similar to regions used for manual measurement), regions of interest (ROIs) were segmented manually by selecting the same region for both NC and PC scans (Fig. 4-g to 4-l). The extracted x, y, and z data were then saved as a comma-separated values (CSV) file. Since the spatial data of the NC and PC scans do not necessarily overlap, nearest (x, y) points in each PC scan to corresponding points of NC scan were found by implementing the N-D nearest point search algorithm (Barber et al., 1996). Next, the NC and PC data were sorted in a descending order based on the height values for each ROI of each sample. Finally, the mean of the top five points, which had the highest value, was calculated as the height value obtained by 3D laser imaging for comparison with that obtained by manual measurement. To find the yolk diameter in both NC and PC scans, points along the axes were selected, yielding the Euclidean distance of those points, and thus, the desired values. The mean value in three readings was recorded as the yolk diameter for NC and PC scans.

2.2.4. Thick albumin's 2D shape analysis

Height's BGR images of samples were subjected to some processing operations to extract some shape features of the thick albumin region (Fig. 5). First, the color channels (B, G, and R) of all images were separated. Then, the yolk part was segmented by setting the pixels with non-maximum intensity value in the R channel to zero, applying an opening operator using a disk shape structural element (radius = 30 pixels), suppressing structures in the image that were lighter than their surrounding and were connected to the image border (clearing image border), and filling holes in the remaining region. Next, the segmented yolk part image was subtracted from the original image. Afterwards, the thick albumin part was segmented by subtracting B channel from G channel of the resulting image, setting the pixels with intensity value lower than 40 to zero, consecutive applying closing and opening operators using disk shape structural elements of radius 30 and 10 pixels, respectively, and filling holes in the remaining region. Finally, six shape descriptors were extracted from the binary image of the segmented thick albumin region, namely, eccentricity (the ratio of the distance between the foci of the ellipse and its major axis length), orientation (the angle between the x-axis and the major axis of the ellipse that has the same second-moments as the region), solidity (the ratio of the area to the convex area), extent (the ratio of the area to the bounding box area), the ratio of long diameter to short diameter, and the ratio of perimeter to area (MATLAB Help Document, 2015). These shape features were then used to develop multilayer perceptron neural networks (MLP-NNs) models for predicting the thick albumin height and the Haugh unit. A further description of the MLP-NNs structure and training process are given in section 3.2.3.

2.3. Software tools

Spectral analysis, N-D nearest point search algorithm, and analysis of the height's BGR images were carried out using MATLAB® R2015b (The MathWorks, Inc., Natick, Massachusetts, USA). The KUKA KR C2 robot control with the KUKA Systems Software V5 (KUKA AG, Germany) along with an in-house built software tool (based on C++, Qt, and the MicroEpsilon scanControl SDK 0.2.0 for Linux) was used for control of

Table 1
Inter-similarity of reflectance spectra of broken egg parts.

Wavelength band (nm)		Yolk[a]	Albumin	Air cell	Shell	Wavelength band (nm)		Yolk	Albumin	Air cell	Shell
400–500	Yolk	0.00 (0.00)				800–900	Yolk	0.00 (0.00)			
	Albumin	0.05 (0.04)	0.00 (0.00)				Albumin	0.01 (0.01)	0.00 (0.00)		
	Air cell	0.03 (0.02)	0.08 (0.07)	0.00 (0.00)			Air cell	0.01 (0.01)	0.02 (0.02)	0.00 (0.00)	
	Shell	0.01 (0.01)	0.05 (0.04)	0.03 (0.02)	0.00 (0.00)		Shell	0.00 (0.00)	0.01 (0.01)	0.01 (0.01)	0.00 (0.00)
500–600	Yolk	0.00 (0.00)				900–1000	Yolk	0.00 (0.00)			
	Albumin	0.05 (0.05)	0.00 (0.00)				Albumin	0.01 (0.01)	0.00 (0.00)		
	Air cell	0.01 (0.00)	0.06 (0.05)	0.00 (0.00)			Air cell	0.02 (0.02)	0.03 (0.03)	0.00 (0.00)	
	Shell	0.00 (0.00)	0.05 (0.05)	0.01 (0.01)	0.00 (0.00)		Shell	0.00 (0.00)	0.01 (0.01)	0.03 (0.02)	0.00 (0.00)
600–700	Yolk	0.00 (0.00)				1000–1100	Yolk	0.00 (0.00)			
	Albumin	0.01 (0.01)	0.00 (0.00)				Albumin	0.00 (0.01)	0.00 (0.00)		
	Air cell	0.00 (0.00)	0.01 (0.01)	0.00 (0.00)			Air cell	0.01 (0.00)	0.00 (0.01)	0.00 (0.00)	
	Shell	0.00 (0.00)	0.01 (0.00)	0.00 (0.00)	0.00 (0.00)		Shell	0.01 (0.01)	0.01 (0.01)	0.01 (0.01)	0.00 (0.00)
700–800	Yolk	0.00 (0.00)				400–1100	Yolk	0.00 (0.00)			
	Albumin	0.01 (0.01)	0.00 (0.00)				Albumin	0.09 (0.09)	0.00 (0.00)		
	Air cell	0.00 (0.00)	0.01 (0.01)	0.00 (0.00)			Air cell	0.05 (0.05)	0.12 (0.11)	0.00 (0.00)	
	Shell	0.00 (0.00)	0.01 (0.01)	0.00 (0.00)	0.00 (0.00)		Shell	0.01 (0.01)	0.08 (0.08)	0.06 (0.05)	0.00 (0.00)

[a] Digits outside and inside the parenthesis are for room and cold storage conditions, respectively.

the robot and to acquire point cloud data. The open-source software CloudCompare 2.10.2 was used for 3D point cloud displaying, processing, and height data extraction from ROIs (Girardeau-Montaut, 2015). The BGR scale images of point clouds were generated for displaying and further processing using 3DTK - The 3D Toolkit (Nüchter et al., 2019) and CloudCompare 2.10.2 (Girardeau-Montaut, 2015), respectively. The MLP-NNs models were developed using the LightScatter toolbox in MATLAB (Mollazade and Arefi, 2017). The mean comparison of the quality traits of samples over the eight assayed cold and room storage time stages as well as the mean comparison between manual and 3D scanning methods in measuring quality traits were carried out by Minitab® 16.2.2 (State College, Pennsylvania, USA) using ANOVAs (one-way) and subsequent post-hoc Tukey's honest significance difference (HSD) tests. MS Excel ver. 2013 (The Microsoft Inc., Redmond, Washington, USA) was used for plotting graphs and calculating statistical measures of correlation coefficient (R), root mean square error (RMSE), and mean absolute percentage error (MAPE).

3. Results and discussion

3.1. Spectroscopy experiment

Fig. 6 provides an overview of the average reflectance of the processed spectra of egg samples (average values of total 225 eggs over the eight storage durations) in which the similarity of spectra of different parts of egg content between the room and cold storage conditions is clearly apparent. In the wavelength range 400–700 nm, which is corresponding to the absorption of light due to color changes, no absorption peak was detected for albumin, yolk, air cell membrane, and eggshell. This means that these egg components are not discolored during storage. On the other hand, in the wavelength region of 950–980 nm, an absorption peak was observed for the albumin part. Albumin is more watery than other parts of the egg. Therefore, due to the vibration of the water molecules (second vibration overtone of water molecule), a higher absorption occurs in this wavelength region (Cen and He, 2007).

The inter-similarity values obtained from the average spectra of different parts of egg content are summarized in Table 1. For the whole wavelength region studied (400–1100 nm), the highest spectral difference was observed between albumin and air cell (0.12 and 0.11 for room and cold storage, respectively). After that, yolk-albumin and shell-albumin with the SAM value of 0.09 and 0.08, respectively, had the highest spectral difference. The highest spectral similarity between different parts of egg content existed in the wavelength region 600–700 and 700–800 nm in which the spectral difference was negligible, with a maximum SAM value of 0.01 for yolk-albumin, air cell-albumin, and shell-albumin. Therefore, from the above mentioned and considering the maximum light reflectance, 600–700 nm was regarded as the most appropriate wavelength region for laser selection for 3D scanning of internal parts of the egg.

3.2. 3D vision experiment

3.2.1. Traits' manual measurements

Results of the manual measurements used to characterize changes in egg quality traits during cold and room storages are shown in Table 2. Overall, no significant changes were observed in egg quality parameters during 21 days of cold storage ($p < 0.05$). The low values of coefficient of variation for Haugh unit (coefficient of variation = 7.61%), yolk index (coefficient of variation = 5.98%), and air cell (coefficient of variation = 13.65%) indicate that storage under controlled temperature and

Table 2
Statistics of manual measurements of egg samples at eight different storage durations.

Type of storage	Day of storage	Mass (g)	Yolk diameter (mm)	Yolk height (mm)	Thick albumin height (mm)	Air cell height (mm)	Haugh unit	Yolk index
Cold storage	0	$57.85^{a} \pm 1.15$	$41.06^{a} \pm 0.99$	$16.69^{c} \pm 0.90$	$5.10^{g} \pm 0.57$	$4.81^{ab} \pm 0.79$	$70.02^{a} \pm 4.97$	$0.41^{b} \pm 0.03$
	3	$57.77^{a} \pm 1.32$	$40.32^{ab} \pm 1.16$	$16.95^{bc} \pm 0.81$	$5.29^{g} \pm 0.65$	$4.25^{b} \pm 0.83$	$71.54^{a} \pm 5.40$	$0.42^{ab} \pm 0.03$
	6	$58.67^{a} \pm 1.59$	$40.49^{ab} \pm 1.22$	$17.03^{abc} \pm 0.59$	$5.05^{g} \pm 0.28$	$5.23^{a} \pm 0.60$	$69.40^{a} \pm 2.45$	$0.42^{ab} \pm 0.02$
	9	$57.61^{a} \pm 1.46$	$39.73^{b} \pm 0.63$	$16.76^{bc} \pm 0.78$	$4.98^{a} \pm 0.62$	$5.46^{a} \pm 0.38$	$68.94^{a} \pm 5.58$	$0.42^{ab} \pm 0.02$
	12	$58.11^{a} \pm 1.56$	$40.09^{ab} \pm 1.08$	$17.38^{abc} \pm 0.73$	$5.40^{g} \pm 0.61$	$5.35^{a} \pm 0.41$	$72.44^{a} \pm 4.93$	$0.43^{a} \pm 0.02$
	15	$58.08^{a} \pm 1.39$	$39.69^{b} \pm 0.99$	$17.58^{ab} \pm 0.70$	$5.41^{a} \pm 0.68$	$5.31^{a} \pm 0.48$	$72.44^{a} \pm 5.66$	$0.44^{a} \pm 0.02$
	18	$58.45^{a} \pm 1.56$	$39.72^{b} \pm 0.84$	$17.33^{abc} \pm 0.97$	$5.31^{a} \pm 0.89$	$5.21^{a} \pm 0.75$	$71.21^{a} \pm 7.65$	$0.44^{a} \pm 0.03$
	21	$57.32^{a} \pm 1.61$	$40.14^{ab} \pm 1.16$	$17.86^{a} \pm 0.43$	$5.36^{a} \pm 0.61$	$5.29^{a} \pm 0.40$	$72.34^{a} \pm 5.26$	$0.45^{a} \pm 0.02$
Coefficient of variation (%)		2.55	2.71	4.81	12.13	13.65	7.61	5.98
Room storage	0	$57.85^{a} \pm 1.15$	$41.06^{d} \pm 0.99$	$16.69^{a} \pm 0.90$	$5.10^{a} \pm 0.57$	$4.81^{d} \pm 0.79$	$70.02^{a} \pm 4.97$	$0.41^{a} \pm 0.03$
	3	$57.49^{a} \pm 1.73$	$41.49^{d} \pm 1.02$	$14.88^{b} \pm 0.68$	$3.87^{b} \pm 0.52$	$5.43^{d} \pm 0.47$	$57.89^{b} \pm 6.02$	$0.36^{b} \pm 0.02$
	6	$57.31^{a} \pm 1.68$	$43.25^{e} \pm 1.21$	$14.24^{b} \pm 0.68$	$3.03^{c} \pm 0.53$	$6.48^{c} \pm 0.72$	$46.94^{c} \pm 9.15$	$0.33^{c} \pm 0.02$
	9	$56.83^{ab} \pm 1.28$	$43.74^{bc} \pm 1.09$	$13.16^{c} \pm 0.67$	$2.65^{cd} \pm 0.51$	$7.13^{c} \pm 1.27$	$41.27^{c} \pm 9.66$	$0.30^{d} \pm 0.02$
	12	$55.43^{bc} \pm 1.25$	$44.85^{ab} \pm 1.51$	$12.73^{cd} \pm 0.67$	$2.84^{cd} \pm 0.44$	$8.39^{b} \pm 0.88$	$45.86^{c} \pm 6.49$	$0.28^{de} \pm 0.02$
	15	$55.44^{bc} \pm 1.53$	$44.96^{ab} \pm 1.90$	$12.06^{de} \pm 0.73$	$2.57^{cd} \pm 0.33$	$9.63^{a} \pm 0.45$	$41.65^{c} \pm 6.30$	$0.27^{ef} \pm 0.03$
	18	$55.66^{bc} \pm 1.22$	$45.32^{a} \pm 1.31$	$12.06^{de} \pm 0.64$	$2.64^{cd} \pm 0.36$	$9.70^{a} \pm 0.90$	$42.57^{c} \pm 6.17$	$0.27^{ef} \pm 0.02$
	21	$54.34^{c} \pm 1.57$	$46.14^{a} \pm 1.76$	$11.43^{e} \pm 0.69$	$2.41^{d} \pm 0.29$	$10.41^{a} \pm 0.90$	$39.94^{c} \pm 4.94$	$0.25^{f} \pm 0.02$
Coefficient of variation (%)		3.24	4.97	13.38	30.65	27.53	24.67	17.80

Data presented mean ± standard deviation of values of 15 samples. For each quality trait, means followed by the different letters are significantly different ($p < 0.05$, one way ANOVA, post-hoc Tukey's HSD test).

humidity conditions results in keeping the freshness of the eggs. Under room storage condition, the thick albumin height, yolk height, Haugh unit, and yolk index decreased sharply with the passage of storage time to around half the initial value after 21 days of storage. This significant decrease ($p < 0.05$) was most evident after three days of storage. The high temperature and low humidity of the ambient resulted in the loss of moisture content of egg and subsequently observing significant differences in egg mass loss during the storage period as a function of its length ($p < 0.05$). This decrease in mass and considerable reduction in thick albumin height resulted in sharper reductions of the Haugh unit during room storage. The decline in albumin height is associated with the evaporation of moisture content and loss of carbon dioxide from the eggs during room storage, resulting in an increase of albumin pH, reduce of the activity of albumin proteins, and decrease in albumin consistency and viscosity (Khan et al., 2013). Also, the progress of the egg deterioration leads to loosening of the fiber structure of the vitelline membrane and a decrease in the strength of the yolk membrane. Since variation in yolk diameter was low (coefficient of variation = 4.97%), the significant change of the yolk index with storage duration was mainly due to the sharp decrease in yolk height (coefficient of variation = 13.38%). Furthermore, the variation in Haugh unit (coefficient of variation = 24.67%), yolk index (coefficient of variation = 17.80%), and air cell (coefficient of variation = 27.53%) of room storage samples across the storage time was considerably much higher than those of the cold storage samples. This suggests that greater changes in the 3D profile should be expected for the samples stored at room condition.

3.2.2. 3D vision measurements

The mean comparison of both methods in measuring internal quality traits of eggs in different days of cold and room storage is shown in Tables 3 and 4, respectively. Results indicated no significant difference between the three measurement methods in room storage for the yolk diameter at all storage times ($p < 0.05$). Similarly, in cold storage condition, the values of NC and PC were statistically the same with respect to the yolk diameter. However, at most storage times (except day 0, 12th, and 24th), a significant difference was observed between manual measurement and NC and PC values ($p < 0.05$). This difference is related to human error caused by the gentle pressure of the Vernier caliper span onto the yolk circumference, resulting in the slight indentation of the egg yolk, because of its elastic nature, and fewer readings of the diameter than the actual values. Yolk height readings of NC and PC scans were statistically similar for all storage days at cold and room conditions. However, manual measurement showed significantly higher values ($p < 0.05$). This over-reading is mainly due to human visual blunders in the precise positioning of the probe tip of the height gauge on the upper surface of the egg yolk. Since the yolk index depends on the yolk's diameter and height, no significant difference was observed between the yolk index values of NC and PC scans (except day 15 of cold storage). Since the diameter and the height of the yolk in the manual measurement were respectively lower and higher than the corresponding values in the 3D measurements, accordingly, the yolk index showed significantly higher values than that of NC and PC scans ($p < 0.05$).

In both cold and room storage conditions, the albumin height values of NC scan were significantly lower than those of manual and PC scan measurements ($p < 0.05$). This is due to the transparency of the albumin and the resulting difficulties for laser-based measurements as mentioned in section 2.2.1. Except on the 0, 3rd, 15th, and 18th day of cold storage and the 6th day of room storage, the manual measurement values were significantly higher than the PC measurement values ($p < 0.05$). The reason for this difference lies in selecting a wider ROI of albumin within 10 cm of the yolk in PC scanning, which is more accurate than picking three points in manual measurement. In both storage conditions, except on the 12th, 15th, and 21st day of room storage, there was no significant difference in Haugh unit values between manual and PC scan measurements. But, due to the lower albumin height values in the NC scan, the Haugh unit values in the NC scan were significantly lower than those

Table 3
Mean comparison of manual and 3D vision methods in measuring internal quality traits of eggs in cold storage condition.

Day of storage	Type of measurement	Yolk diameter (mm)	Yolk height (mm)	Thick albumin height (mm)	Air cell height (mm)	Haugh unit	Yolk index
0	Manual	$41.06^{a} \pm 0.99$	$16.69^{a} \pm 0.90$	$5.10^{a} \pm 0.57$	$4.81^{a} \pm 0.79$	$70.02^{a} \pm 4.97$	$0.41^{a} \pm 0.03$
	NC scan	$42.13^{a} \pm 1.85$	$15.88^{b} \pm 0.56$	$1.81^{b} \pm 0.90$	$4.69^{a} \pm 0.55$	$20.74^{b} \pm 16.74$	$0.38^{b} \pm 0.02$
	PC scan	$41.35^{a} \pm 1.37$	$16.31^{ab} \pm 0.67$	$4.75^{a} \pm 0.72$	$4.75^{a} \pm 0.56$	$66.61^{a} \pm 6.69$	$0.40^{ab} \pm 0.02$
3	Manual	$40.32^{b} \pm 1.16$	$16.95^{a} \pm 0.81$	$5.29^{a} \pm 0.65$	$4.25^{a} \pm 0.83$	$71.54^{a} \pm 5.40$	$0.42^{a} \pm 0.03$
	NC scan	$42.19^{a} \pm 1.59$	$15.86^{b} \pm 0.67$	$1.92^{b} \pm 0.59$	$4.70^{a} \pm 0.97$	$25.40^{b} \pm 12.14$	$0.38^{b} \pm 0.02$
	PC scan	$41.42^{ab} \pm 1.63$	$16.18^{b} \pm 0.74$	$4.96^{a} \pm 0.99$	$4.87^{a} \pm 0.81$	$68.33^{a} \pm 8.10$	$0.39^{b} \pm 0.03$
6	Manual	$40.49^{b} \pm 1.22$	$17.03^{a} \pm 0.59$	$5.05^{a} \pm 0.28$	$5.23^{a} \pm 0.60$	$69.40^{a} \pm 2.45$	$0.42^{a} \pm 0.02$
	NC scan	$42.75^{a} \pm 1.55$	$16.01^{b} \pm 0.55$	$1.73^{c} \pm 0.76$	$4.97^{a} \pm 0.76$	$18.71^{b} \pm 13.27$	$0.38^{b} \pm 0.02$
	PC scan	$42.39^{a} \pm 1.60$	$16.32^{b} \pm 0.55$	$4.59^{b} \pm 0.39$	$5.07^{a} \pm 0.67$	$65.11^{a} \pm 3.51$	$0.39^{b} \pm 0.02$
9	Manual	$39.73^{b} \pm 0.63$	$16.76^{a} \pm 0.78$	$4.98^{a} \pm 0.62$	$5.46^{a} \pm 0.38$	$68.94^{a} \pm 5.58$	$0.42^{a} \pm 0.02$
	NC scan	$41.76^{a} \pm 1.12$	$15.95^{b} \pm 0.62$	$1.62^{c} \pm 0.93$	$5.47^{a} \pm 0.39$	$15.51^{b} \pm 17.27$	$0.38^{b} \pm 0.02$
	PC scan	$41.21^{a} \pm 1.00$	$16.22^{ab} \pm 0.61$	$4.20^{b} \pm 0.62$	$5.57^{a} \pm 0.36$	$61.37^{a} \pm 6.72$	$0.39^{b} \pm 0.02$
12	Manual	$40.09^{a} \pm 1.08$	$17.38^{a} \pm 0.73$	$5.40^{a} \pm 0.61$	$5.35^{a} \pm 0.41$	$72.44^{a} \pm 4.93$	$0.43^{a} \pm 0.02$
	NC scan	$41.35^{a} \pm 1.78$	$16.22^{b} \pm 0.75$	$1.83^{c} \pm 1.00$	$5.30^{a} \pm 0.61$	$20.82^{b} \pm 16.12$	$0.39^{b} \pm 0.02$
	PC scan	$40.76^{a} \pm 1.42$	$16.57^{b} \pm 0.73$	$4.69^{b} \pm 0.57$	$5.45^{a} \pm 0.60$	$66.13^{a} \pm 5.33$	$0.41^{b} \pm 0.02$
15	Manual	$39.69^{b} \pm 0.99$	$17.58^{a} \pm 0.70$	$5.41^{a} \pm 0.68$	$5.31^{a} \pm 0.48$	$72.44^{a} \pm 5.66$	$0.44^{a} \pm 0.02$
	NC scan	$41.35^{a} \pm 1.30$	$16.30^{b} \pm 0.59$	$2.01^{b} \pm 0.84$	$5.28^{a} \pm 0.47$	$25.69^{b} \pm 16.04$	$0.39^{c} \pm 0.02$
	PC scan	$40.56^{ab} \pm 1.09$	$16.77^{b} \pm 0.66$	$5.02^{a} \pm 0.68$	$5.42^{a} \pm 0.48$	$69.03^{a} \pm 6.21$	$0.41^{b} \pm 0.02$
18	Manual	$39.72^{b} \pm 0.84$	$17.33^{a} \pm 0.97$	$5.31^{a} \pm 0.89$	$5.21^{a} \pm 0.75$	$71.21^{a} \pm 7.65$	$0.44^{a} \pm 0.03$
	NC scan	$40.95^{a} \pm 0.84$	$16.47^{b} \pm 0.84$	$1.52^{b} \pm 0.36$	$5.16^{a} \pm 0.89$	$13.84^{b} \pm 14.30$	$0.40^{b} \pm 0.02$
	PC scan	$40.57^{a} \pm 0.74$	$16.90^{ab} \pm 0.87$	$4.71^{a} \pm 1.01$	$5.42^{a} \pm 0.79$	$65.43^{a} \pm 10.03$	$0.42^{ab} \pm 0.02$
21	Manual	$40.14^{a} \pm 1.16$	$17.86^{a} \pm 0.43$	$5.36^{a} \pm 0.61$	$5.29^{a} \pm 0.40$	$72.34^{a} \pm 5.26$	$0.45^{a} \pm 0.02$
	NC scan	$40.63^{a} \pm 0.79$	$16.49^{b} \pm 0.46$	$2.22^{c} \pm 1.01$	$5.41^{a} \pm 0.51$	$30.63^{b} \pm 17.04$	$0.41^{b} \pm 0.02$
	PC scan	$40.83^{a} \pm 0.99$	$16.82^{b} \pm 0.50$	$4.62^{b} \pm 0.63$	$5.50^{a} \pm 0.49$	$65.72^{a} \pm 6.36$	$0.41^{b} \pm 0.02$

Data presented mean ± standard deviation of values of 15 samples. For each quality trait in each storage time, means followed by the different letters are significantly different ($p < 0.05$, one way ANOVA, post-hoc Tukey's HSD test). NC and PC stand for no coating and powder coating, respectively.

obtained by the others ($p < 0.05$). The results also indicated no significant difference between the three methods in measuring the air cell height during cold and room storage ($p < 0.05$).

Fig. 7 shows the linearity and error measures between the manual and the 3D scanning methods in measuring the quality traits of different parts of egg content with the whole data set of cold and room storage conditions. According to the results obtained, it can be stated that without coating, the yolk diameter, yolk height, yolk index, and air cell height could be reliably measured using 3D laser scanning. For these quality traits, high linearity ($R > 0.93$) and very low error (MAPE < 3.21) were observed between NC scan and PC scan. Furthermore, in manual measurement vs. NC scan, the lowest correlation coefficient and

Table 4
Mean comparison of manual and 3D vision methods in measuring internal quality traits of eggs in room storage condition.

Day of storage	Type of measurement	Yolk diameter (mm)	Yolk height (mm)	Thick albumin height (mm)	Air cell height (mm)	Haugh unit	Yolk index
0	Manual	$41.06^{a} \pm 0.99$	$16.69^{a} \pm 0.90$	$5.10^{a} \pm 0.57$	$4.81^{a} \pm 0.79$	$70.02^{a} \pm 4.97$	$0.41^{a} \pm 0.03$
	NC scan	$42.13^{a} \pm 1.85$	$15.88^{b} \pm 0.56$	$1.81^{b} \pm 0.90$	$4.69^{a} \pm 0.55$	$20.74^{b} \pm 16.74$	$0.38^{b} \pm 0.02$
	PC scan	$41.35^{a} \pm 1.37$	$16.31^{ab} \pm 0.67$	$4.75^{a} \pm 0.72$	$4.75^{a} \pm 0.56$	$66.61^{a} \pm 6.69$	$0.40^{ab} \pm 0.02$
3	Manual	$41.49^{a} \pm 1.02$	$14.88^{a} \pm 0.68$	$3.87^{a} \pm 0.52$	$5.43^{a} \pm 0.47$	$57.89^{a} \pm 6.02$	$0.36^{a} \pm 0.02$
	NC scan	$42.11^{a} \pm 1.05$	$14.34^{b} \pm 0.51$	$1.27^{c} \pm 0.50$	$5.70^{a} \pm 0.59$	$6.23^{b} \pm 15.81$	$0.34^{b} \pm 0.01$
	PC scan	$41.86^{a} \pm 1.01$	$14.62^{ab} \pm 0.54$	$3.29^{b} \pm 0.58$	$5.79^{a} \pm 0.64$	$50.50^{a} \pm 7.83$	$0.35^{ab} \pm 0.01$
6	Manual	$43.25^{a} \pm 1.21$	$14.24^{a} \pm 0.68$	$3.03^{a} \pm 0.53$	$6.48^{a} \pm 0.72$	$46.94^{a} \pm 9.15$	$0.33^{a} \pm 0.02$
	NC scan	$44.17^{a} \pm 1.61$	$13.16^{b} \pm 0.52$	$0.91^{b} \pm 0.34$	$6.62^{a} \pm 1.15$	$-8.07^{b} \pm 14.46$	$0.30^{b} \pm 0.02$
	PC scan	$44.08^{a} \pm 1.68$	$13.35^{b} \pm 0.61$	$2.76^{a} \pm 0.55$	$6.65^{a} \pm 1.11$	$42.83^{a} \pm 8.27$	$0.30^{b} \pm 0.02$
9	Manual	$43.74^{a} \pm 1.09$	$13.16^{a} \pm 0.67$	$2.65^{a} \pm 0.51$	$7.13^{a} \pm 1.27$	$41.27^{a} \pm 9.66$	$0.30^{a} \pm 0.02$
	NC scan	$44.66^{a} \pm 1.16$	$12.31^{b} \pm 0.56$	$0.64^{c} \pm 0.22$	$7.31^{a} \pm 1.66$	$-24.31^{b} \pm 22.05$	$0.28^{b} \pm 0.01$
	PC scan	$44.58^{a} \pm 1.38$	$12.52^{b} \pm 0.59$	$2.19^{b} \pm 0.60$	$7.41^{a} \pm 1.66$	$31.60^{a} \pm 15.34$	$0.28^{b} \pm 0.02$
12	Manual	$44.85^{a} \pm 1.51$	$12.73^{a} \pm 0.67$	$2.84^{a} \pm 0.44$	$8.39^{a} \pm 0.88$	$45.86^{a} \pm 6.49$	$0.28^{a} \pm 0.02$
	NC scan	$45.86^{a} \pm 1.63$	$11.49^{b} \pm 0.64$	$0.68^{c} \pm 0.27$	$8.88^{a} \pm 1.27$	$-15.29^{c} \pm 13.33$	$0.25^{b} \pm 0.02$
	PC scan	$46.09^{a} \pm 1.69$	$11.76^{b} \pm 0.68$	$2.26^{b} \pm 0.56$	$9.00^{a} \pm 1.36$	$35.48^{b} \pm 9.53$	$0.26^{b} \pm 0.02$
15	Manual	$44.96^{a} \pm 1.90$	$12.06^{a} \pm 0.73$	$2.57^{a} \pm 0.33$	$9.63^{b} \pm 0.45$	$41.65^{a} \pm 6.30$	$0.27^{a} \pm 0.03$
	NC scan	$45.83^{a} \pm 1.58$	$10.96^{b} \pm 0.69$	$0.56^{c} \pm 0.59$	$10.47^{a} \pm 0.89$	$-30.82^{c} \pm 27.27$	$0.24^{b} \pm 0.02$
	PC scan	$46.03^{a} \pm 1.83$	$11.22^{b} \pm 0.68$	$1.70^{b} \pm 0.53$	$10.61^{a} \pm 0.92$	$22.70^{b} \pm 13.46$	$0.24^{b} \pm 0.02$
18	Manual	$45.32^{a} \pm 1.31$	$12.06^{a} \pm 0.64$	$2.64^{a} \pm 0.36$	$9.70^{a} \pm 0.90$	$42.57^{a} \pm 6.17$	$0.27^{a} \pm 0.02$
	NC scan	$46.50^{a} \pm 1.63$	$10.86^{b} \pm 0.54$	$0.70^{c} \pm 0.46$	$10.23^{a} \pm 1.26$	$-18.74^{b} \pm 23.00$	$0.23^{b} \pm 0.02$
	PC scan	$46.62^{a} \pm 1.44$	$11.16^{b} \pm 0.59$	$2.05^{b} \pm 0.54$	$10.38^{a} \pm 1.31$	$30.63^{a} \pm 12.29$	$0.24^{b} \pm 0.02$
21	Manual	$46.14^{a} \pm 1.76$	$11.43^{a} \pm 0.69$	$2.41^{a} \pm 0.29$	$10.41^{a} \pm 0.90$	$39.94^{a} \pm 4.94$	$0.25^{a} \pm 0.02$
	NC scan	$47.19^{a} \pm 1.78$	$10.41^{b} \pm 0.39$	$0.53^{c} \pm 0.14$	$11.34^{a} \pm 1.31$	$-20.03^{c} \pm 8.41$	$0.22^{b} \pm 0.01$
	PC scan	$46.92^{a} \pm 1.78$	$10.62^{b} \pm 0.38$	$1.85^{b} \pm 0.44$	$11.45^{a} \pm 1.40$	$28.50^{b} \pm 9.11$	$0.23^{b} \pm 0.01$

Data presented mean ± standard deviation of values of 15 samples. For each quality trait in each storage time, means followed by the different letters are significantly different ($p < 0.05$, one way ANOVA, post-hoc Tukey's HSD test). NC and PC stand for no coating and powder coating, respectively.

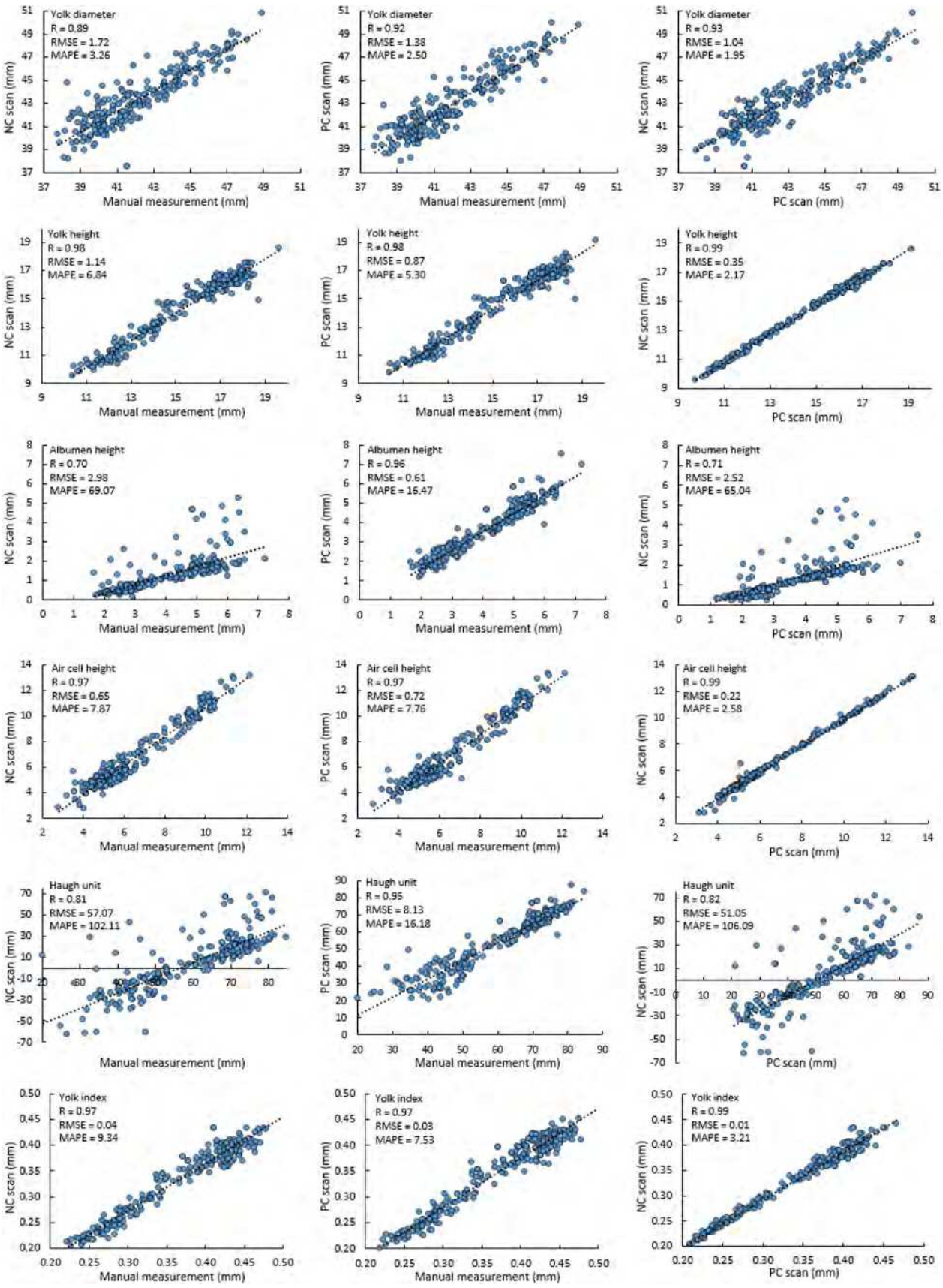

Fig. 7. Linearity and error measures between manual and 3D scanning methods.

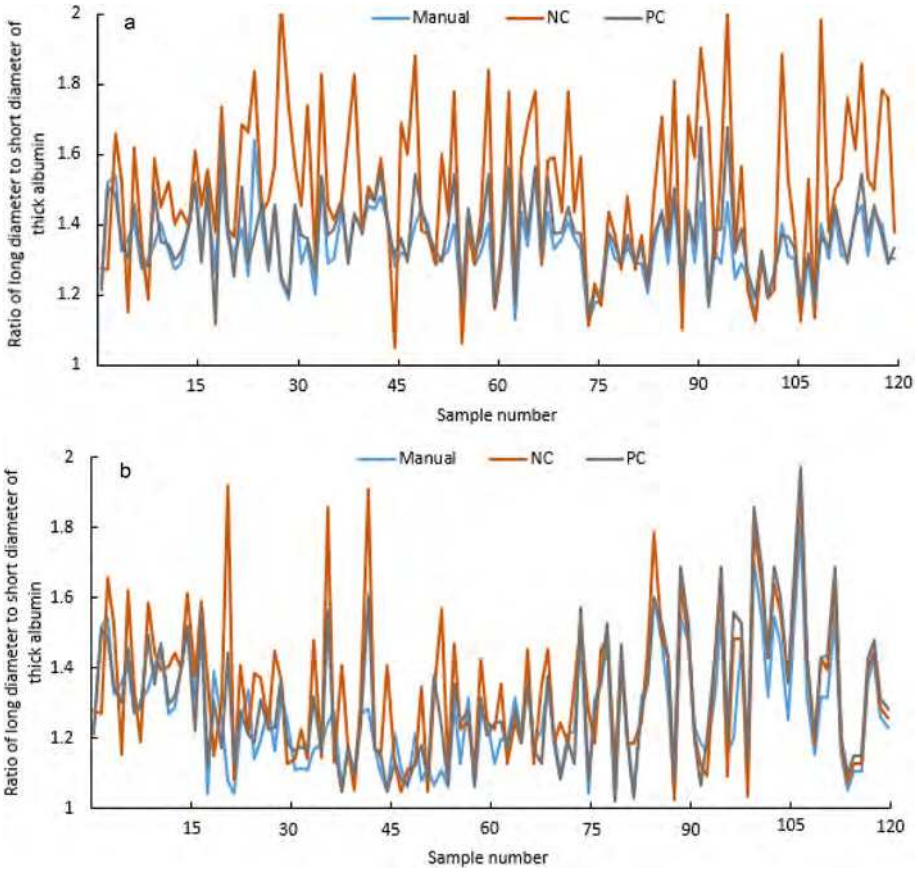

Fig. 8. Ratio of thick albumin's long diameter to its short diameter for samples stored at cold (a) and room storage (b) conditions. NC and PC stand for no coating and powder coating, respectively.

the highest MAPE were 0.89 and 9.34 for yolk diameter and yolk index, respectively. Despite the strong linear relationship ($R = 0.96$) and relatively low error rate (MAPE = 16.47) between the manual method and PC scan in measuring the albumin height, results obtained by the NC scan were disappointing ($R < 0.71$ and MAPE > 65.04). Since the change in the Haugh unit is mostly influenced by the change in albumin height, similar disappointing results were observed in measuring Haugh unit by NC scan ($R < 0.82$ and MAPE > 102.11). Taking all of the above into account, it can be stated that the 3D laser scanning is proposed to measure the Haugh unit only if the albumin portion near the yolk is covered with a thin layer of Talcum powder.

3.2.3. Thick albumin's 2D shape analysis

Fig. 8 shows the ratio of the thick albumin's long diameter to its short diameter for samples stored at different storage conditions. As observed, for both cold and room storage samples, the manual and PC scan measurement curves approximately fit each other. The R and mean absolute error (MAE) values were 0.86 and 0.04 in cold storage and 0.89 and 0.07 in room storage for manual vs. PC scan measurements, respectively. The NC scan method has failed to provide values close to those of the manual and PC scan methods, especially for cold storage samples (Fig. 8). For manual vs. NC scan and PC scan vs. NC scan measurements, the R and MAE values were obtained as 0.59 and 0.18, and 0.61 and 0.16 in cold storage and 0.67 and 0.12, and 0.83 and 0.08 in room storage condition, respectively. Since the measurement of thick albumin height by the NC scan method was highly error-prone (Fig. 7), the analysis of BGR images derived from height values was not suitable for distinguishing the thick albumin from the thin albumin, resulting in different amounts of thick albumin's long diameter to its short diameter ratio compared to those of manual and PC scan methods.

Based on the extracted 2D shape features of BGR images of the PC scan method (including eccentricity, orientation, solidity, extent, the ratio of long diameter to short diameter, and the ratio of perimeter to area) and measured thick albumin height and Haugh unit values, the MLP-NNs models with one hidden layer were developed to predict the thick albumin height and Haugh unit. After merging cold and room storage datasets, to avoid over-fitting and to ensure the prediction results truly represent the models' performance, the resulting dataset was randomly split into three separate parts: 65% for training, 15% for cross-validation, and the rest for testing phase. The number of neurons in the hidden layer was changed and the performance of models was evaluated by calculating R, RMSE, and MAPE in the training and cross-validation stages. For all developed NNs models, the learning algorithm, the transfer function of the hidden layer, the transfer function of the output layer, and the learning rate were Levenberg-Marquardt, tangent sigmoid, linear, and 0.1, respectively. According to the results obtained in 50 replicates, the models with two neurons in the hidden layer exhibited the highest R and lowest RMSE and MAPE values and were the most appropriate structure for predicting thick albumin height and Haugh unit. Performance results of the best MLP-NNs models for predicting thick albumin height and Haugh unit are presented in Fig. 9. The corresponding R, RMSE, and MAPE of the best models in the testing stage were 0.84, 0.63, and 9.82 for albumin height prediction, and 0.84, 6.53, and 8.16 for Haugh unit prediction, respectively. These results demonstrate good agreement between the predicted and desired values.

4. Conclusions

In this research, a high-precision robot and laser scanner were used to obtain high-resolution 3D point clouds. This was done to carefully examine the feasibility of using 3D laser imaging technology for measuring the internal quality traits of the egg. Results showed that

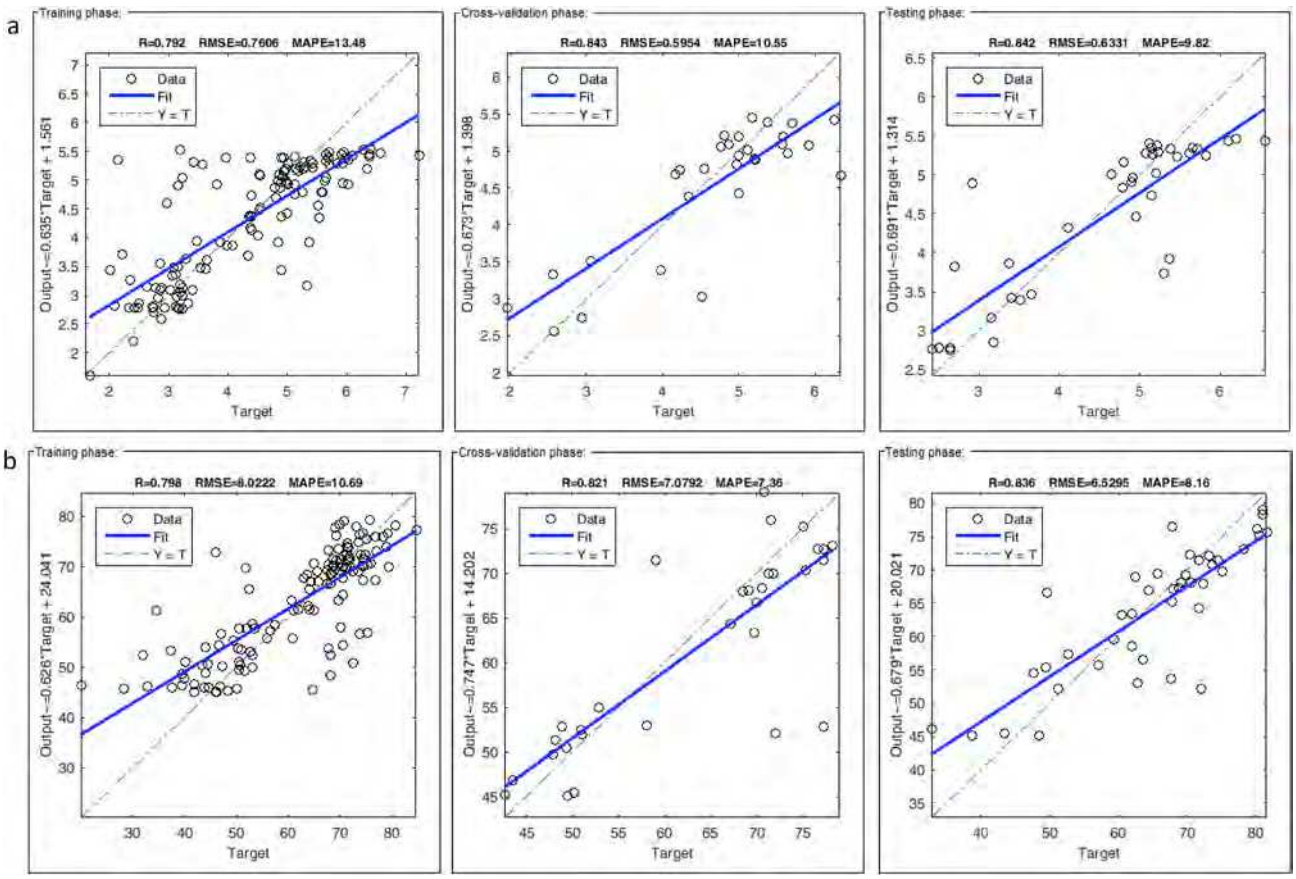

Fig. 9. Performance measures of ANN models in prediction of thick albumin height (a) and Haugh unit (b) using 2D shape features.

without covering the egg content, it is possible to accurately measure yolk index and air cell height. On the other hand, to measure thick albumin height and Haugh unit accurately, coverage the albumin region with Talcum powder before scanning is required. As an alternative, the thick albumin height and Haugh unit can be successfully predicted by processing 2D images of the thick albumin region and the usage of fully trained MLP-NNs models. For industrial applications, a combination of a moving table, a linear laser diode, and a conventional camera can be used to acquire 3D data at an affordable price. The practical outcome of this research will lead to developing a new instrument relevant to the quality control laboratories of the egg production farms and the food industry. The 3D scanning system coupled with a conventional 2D imaging camera could also be installed on the egg processing machines, which are used for separating egg content after cracking, based on their freshness using yolk index and Haugh unit criteria.

CRediT authorship contribution statement

Kaveh Mollazade: Conceptualization, Methodology, Investigation, Formal analysis, Resources, Writing - original draft. **Sven Jörissen:** Software, Validation, Visualization, Writing - review & editing. **Andreas Nüchter:** Supervision, Project administration, Funding acquisition, Writing - review & editing.

Declaration of competing interest

The authors declare that they have no known competing financial interests or personal relationships that could have appeared to influence the work reported in this paper.

Acknowledgements

The authors are grateful to the German Research Foundation (DFG-Deutsche Forschungsgemeinschaft) for financial support through the grant number NU 230/11-1 for project number 423765662. Thanks also go to the Vice-Chancellor for Research office of the University of Kurdistan, Iran. The authors would also like to show their gratitude to Michael Bleier and Dorit Borrmann for their technical advice.

Appendix A. Supplementary data

Supplementary data to this article can be found online at https://doi.org/10.1016/j.jfoodeng.2020.110289.

References

Abdel-Nour, N., 2008. Chicken Egg Quality Assessment from Visible/near Infrared Observations. M.Sc. thesis. McGill University, Canada.
Abeyrathne, E.D.N.S., Lee, H.Y., Ahn, D.U., 2013. Egg white proteins and their potential use in food processing or as nutraceutical and pharmaceutical agents-A review. Poultry Sci. 92, 3292–3299.
Aboonajmi, M., Akram, A., Nishizu, T., Kondo, N., Setarehdan, S.K., Rajabipour, A., 2010. An ultrasound based technique for the determination of poultry egg quality. Res. Agric. Eng. 56 (1), 26–32.
Aygun, A., Sert, D., 2013. Effects of vacuum packing on eggshell microbial activity and egg quality in table eggs under different storage temperatures. J. Sci. Food Agric. 93 (7), 1626–1632.
Barber, C.B., Dobkin, D.P., Huhdanpaa, H.T., 1996. The quickhull algorithm for convex hulls. ACM Trans. Math Software 22 (4), 469–483.
Cen, H., He, Y., 2007. Theory and application of near infrared reflectance spectroscopy in determination of food quality. Trends Food Sci. Technol. 18 (2), 72–83.
Girardeau-Montaut, D., 2015. Cloud Compare - 3d Point Cloud and Mesh Processing Software. Open Source Project.
Huang, Q., Qiu, N., Ma, M.H., Jin, Y.G., Yang, H., Geng, F., Sun, S.H., 2012. Estimation of egg freshness using S-ovalbumin as an indicator. Poultry Sci. 91 (3), 739–743.

Ivorra, E., Sánchez, A.J., Camarasa, J.G., Diago, M.P., Tardaguila, J., 2015. Assessment of grape cluster yield components based on 3D descriptors using stereo vision. Food Contr. 50, 273–282.

Khan, M.J.A., Khan, S.H., Bukhsh, A., Abbass, M.I., Javed, M., 2013. Effect of different storage period on egg weight, internal egg quality and hatchability characteristics of Fayumi eggs. Ital. J. Anim. Sci. 12 (e51), 323–328.

Kjaer, K.H., Ottosen, C.O., 2015. 3D laser triangulation for plant phenotyping in challenging environments. Sensors 15, 13533–13547.

Lazaros, N., Sirakoulis, G.C., Gasteratos, A., 2008. Review of stereo vision algorithms: from software to hardware. Int. J. Optomechatronics 2 (4), 435–462.

Lee, D.J., Lane, R.M., Chang, G.H., 2001. Three-dimensional reconstruction for high-speed volume measurement. In: Proc. SPIE 4189, Machine Vision and Three-Dimensional Imaging Systems for Inspection and Metrology. https://doi.org/10.1117/12.417201.

Ma, D., Liu, J., Huang, J., Li, H., Liu, P., Chen, H., Qian, J., 2016. Spectral similarity assessment based on a spectrum reflectance-absorption index and simplified curve patterns for hyperspectral remote sensing. Sensors 16 (2), 152. https://doi.org/10.3390/s16020152.

Mathiassen, J.R., Misimi, E., Toldnes, B., Bondø, M., Ostvik, S.O., 2011. High-speed weight estimation of whole herring (Clupea harengus) using 3D machine vision. J. Food Sci. 76 (6), E458–E464.

MATLAB Help Document, 2015. Image Processing Toolbox User's Guide. MathWorks, Inc., Natick, MA, USA.

Miranda, J.M., Anton, X., Redondo-Valbuena, C., Roca-Saavedra, P., Rodriguez, J.A., Lamas, A., Frqanco, C.M., Cepeda, A., 2015. Egg and egg-derived foods: effects on human health and use as functional foods. Nutrients 7 (1), 706–729.

Mollazade, K., Arefi, A., 2017. *LightScatter*: a comprehensive software package for non-destructive monitoring of horti-food products by monochromatic imaging-based spatially-resolved light scattering technology. Comput. Electron. Agric. 142 (B), 597–606.

Moomkesh, Sh, Mireei, S.A., Sadeghi, M., Nazeri, M., 2017. Early detection of freezing damage in sweet lemons using Vis/SWNIR spectroscopy. Biosyst. Eng. 164, 157–170.

Nüchter, A., et al., 2019. 3DTK - the 3D Toolkit. http://threedtk.de/.

Sakai, N., Yonekawa, S., 1992. Three-dimensional image analysis of the shape of soybean seed. J. Food Eng. 15 (3), 221–234.

Sture, O., Oye, E.R., Skavhaug, A., Mathiassen, J.R., 2016. A 3D machine vision system for quality grading of Atlantic salmon. Comput. Electron. Agric. 123, 142–148.

Suktanarak, S., Teerachaichayut, S., 2017. Non-destructive quality assessment of hens' eggs using hyperspectral images. J. Food Eng. 215, 97–103.

Tippetts, B., Lee, D.Y., Lillywhite, K., Archibald, J., 2016. Review of stereo vision algorithms and their suitability for resource-limited systems. J. Real-Time Image Process. 11 (1), 5–25.

Verdú, S., Ivorra, E., Sánchez, A.J., Girón, J., Barat, J.M., Grau, R., 2013. Comparison of TOF and SL techniques for in-line measurement of food item volume using animal and vegetable tissues. Food Contr. 33 (1), 221–226.

Yao, K., Sun, J., Zhou, X., Nirere, A., Tian, Y., Wu, X., 2020. Nondestructive detection for egg freshness grade based on hyperspectral imaging technology. J. Food Process. Eng. https://doi.org/10.1111/jfpe.13422.

Zhang, W., Pan, L., Tu, S., Zhan, G., Tu, K., 2015. Non-destructive internal quality assessment of eggs using a synthesis of hyperspectral imaging and multivariate analysis. J. Food Eng. 157, 41–48.

Zou, Y., Chen, T., 2018. Laser vision seam tracking system based on image processing and continuous convolution operator tracker. Optic Laser. Eng. 105, 141–149.